SEISMIC ENERGY EVALUATION IN 3D FRICTION PENDULUM SYSTEMS UNDER EXTREME GROUND MOTIONS

N. D. Oliveto [(1)]

[(1)] *Researcher, Department of Civil and Architectural Engineering, University of Catania, noliveto@buffalo.edu*

Abstract

Seismic isolation is nowadays a widely adopted technology for the protection of building infrastructure from earthquakes. One of the most effective and extensively used seismic protection devices is the friction pendulum (FP) system. While it is common practice to analyze the behavior of FP systems based on the principle of a linearized 1D pendulum motion, more sophisticated 2D or 3D models are preferred under bi-directional or even tri-directional ground motions, considering the motion of a mass sliding with friction on a sphere. In a companion paper published in the 2020 proceedings of this conference, a computational model was developed for the analysis of the three-dimensional motion of FP systems and used in the simulation of the response of such systems under tri-directional near-fault and long-period ground motions. The results were presented in the form of displacement response spectra for several values of the friction coefficient. In the present work, those results are extended to include base shear, residual displacements and distance traveled by the slider. Moreover, a comprehensive view of the demands posed by the selected extreme ground motions is provided in terms of seismic energy spectra.

Keywords: seismic isolation; friction pendulum; long-period ground motions; seismic energy; nonlinear modeling.

1. Introduction

Although considerable attention has been devoted in the recent past to the effects of near-fault and long-period earthquakes on tall buildings and base-isolated structures, not much has been said regarding the resonant effects of nearly periodic ground motions on friction pendulum systems. Unlike systems with viscous damping, classical friction-damped linear systems can exhibit an unbounded response at resonance [1-4]. Recent work by this author [5] shows that when the nonlinear geometry of the spherical surfaces is considered, although bounded, the response of FP systems can still be unreasonably large.

In a companion manuscript, published in the 2020 proceedings of this conference [6], a novel three-dimensional formulation was presented illustrating the geometrically nonlinear motion of a mass sliding with friction on a sphere and used for the response simulation of FP systems under tri-directional near-fault and long-period ground motions. The results, presented in the form of response spectra for several values of the friction coefficient, showed displacement demands exceeding by far the capacity of the isolation devices in a wide range of periods. Moreover, it was seen that strong vertical ground accelerations can potentially determine the compression force on the devices to vanish with consequent uplift of the superstructure.

The objective of this paper is to extend the results presented in the companion manuscript [6] to include additional response quantities that are important for assessing the performance and safety of base-isolated structures, namely base shear, residual displacement, seismic input energy and distance traveled by the FP slider.

2. Governing equations

As described in [6], the equations of motion of the friction pendulum system under earthquake excitation may be written as

$$
\begin{aligned}
&m\left(\ddot{\mathbf{r}}_h+\ddot{\mathbf{r}}_{hg}\right)+\mathbf{F}_h=\mathbf{0}\\
&m\left(\ddot{z}_g+\ddot{z}+g\right)+V=0
\end{aligned}
\tag{1}
$$

where m is the mass of the superstructure, $\mathbf{r}_h=x\mathbf{e}_x+y\mathbf{e}_y$ is the vector of horizontal displacements relative to the ground, z is the vertical displacement relative to the ground, $\mathbf{F}_h=H_x\mathbf{e}_x+H_y\mathbf{e}_y$ is the vector of horizontal forces, V is the vertical force, $\ddot{\mathbf{r}}_{hg}$ is the vector of horizontal ground accelerations, $\ddot{z}_g$ is the vertical ground acceleration, and g is the acceleration of gravity. For further details on geometry, kinematics and equilibrium of the system considered, the reader is referred to [6].

2.1 Energy quantities

Multiplying the first and second of Eqs. (1) by relative velocities $\dot{\mathbf{r}}_h$ and $\dot{z}$ respectively, and integrating with respect to time leads to

$$
\begin{aligned}
&\int_0^t m\ddot{\mathbf{r}}_h\cdot\dot{\mathbf{r}}_h d\tau+\int_0^t \mathbf{F}_h\cdot\dot{\mathbf{r}}_h d\tau=-\int_0^t m\ddot{\mathbf{r}}_{hg}\cdot\dot{\mathbf{r}}_h d\tau\\
&\int_0^t m\ddot{z}\dot{z}d\tau+\int_0^t V\dot{z}d\tau+\int_0^t mg\dot{z}d\tau=-\int_0^t m\ddot{z}_g\dot{z}d\tau
\end{aligned}
\tag{2}
$$

The right sides of these equations provide the horizontal and vertical energy input to the system since the beginning of the ground motion:

$$
E_I(t)=-\int_0^t m\ddot{\mathbf{r}}_{hg}\cdot\dot{\mathbf{r}}_h d\tau-\int_0^t m\ddot{z}_g\dot{z}d\tau \tag{3}
$$

The sum of the first terms on the left sides of Eqs. (2) gives the kinetic energy of the mass associated with its motion relative to the ground:

$$
E_K(t)=\int_0^t m\ddot{\mathbf{r}}_h\cdot\dot{\mathbf{r}}_h d\tau+\int_0^t m\ddot{z}\dot{z}d\tau=\frac{1}{2}m\left(\dot{\mathbf{r}}_h\cdot\dot{\mathbf{r}}_h\right)+\frac{1}{2}m\dot{z}^2 \tag{4}
$$

The sum of the second terms on the left sides of Eqs. (2) provides the sum of the energy dissipated by friction, E_F, and the recoverable strain energy, E_S, of the system:

$$
E_F(t)+E_S(t)=\int_0^t \mathbf{F}_h\cdot\dot{\mathbf{r}}_h d\tau+\int_0^t V\dot{z}d\tau \tag{5}
$$

Finally, the third term on the left side of the second of Eqs. (2) is the potential energy of the mass:

$$
E_W(t)=\int_0^t mg\dot{z}d\tau=mgz(t) \tag{6}
$$

© The 17th World Conference on Earthquake Engineering

2.2 Stop and go motion

During an earthquake, friction-based systems can alternate phases of motion to phases of standstill, depending on the relative magnitudes of ground acceleration and friction. Let us introduce a local coordinate system defined by unit vectors $\mathbf{e}_N = -\mathbf{e}_R$ (normal to the sliding surface), $\mathbf{e}_M$ (tangent to the meridian identified by $\mathbf{e}_R$ and $\mathbf{r}_h$), and $\mathbf{e}_P = \mathbf{e}_M \times \mathbf{e}_N$ (tangent to the parallel at the position considered). Then, the reaction of the sliding surface may be written as

$$\mathbf{R} = R_N \mathbf{e}_N + R_M \mathbf{e}_M + R_P \mathbf{e}_P = R_N \mathbf{e}_N + R_T \mathbf{e}_T \tag{7}$$

For motion to be initiated the following condition needs to be satisfied

$$R_T \geq \mu_{st} R_N \tag{8}$$

where μ_{st} is the static friction coefficient.

3. Earthquake simulations

In [6], Eqs. (1) were solved for the nearly periodic, near-fault and long-period recorded ground motions listed in Table 1. The pseudo-velocity response spectra for the three components of each ground motion and a damping ratio ζ=0.05 are plotted in Fig.1. We note pseudo-velocities considerably higher than those prescribed in seismic building codes. The first ground motion, recorded at station SCT (Secretaria de Communicaciones y Transportes) during the 1985 Mexico City earthquake was downloaded from the IIUNAM's Strong Motion Network (RAII-UNAM) operated at the Institute of Engineering of the National Autonomous University of México. The second and third, recorded during the 2007 Chuetsu-Oki and the 2008 Iwate-Miyagi Nairiku earthquakes respectively, were retrieved from the NIED (National Research Institute for Earth Science and Disaster Resilience, Japan) strong-motion seismograph network K-NET. Finally, the fourth ground motion, recorded at El Centro during the 1979 Imperial Valley earthquake, was downloaded from the COSMOS (Consortium for Strong-Motion Observation Systems) Strong Motion Virtual Data Center (VDC). Table 1 includes the epicentral distance, e_d, and the strong motion duration, t_d, for each of the ground motions considered. The latter were computed based on the definition of strong motion duration given by Trifunac and Brady [7]. This is given by

$$t_d = T_{0.95} - T_{0.05} \tag{9}$$

where $T_{0.95}$ and $T_{0.05}$ are the times at which 95% and 5% of the accelerogram's total energy are reached. For the determination of the strong motion durations listed in Table 1, the cumulative ground acceleration energy was computed as

$$E(t) = \int_0^t \left(\left\| \ddot{\mathbf{r}}_{hg} \right\|^2 + \ddot{z}_g^2 \right) d\tau \tag{10}$$

The two horizontal components and the vertical component of each ground motion were applied simultaneously. The analyses were carried out for a wide range of periods of the isolation system and the results were presented in the form of displacement response spectra for different values of the dynamic friction coefficient, μ. Due to a very strong vertical component of ground acceleration, the compression forces on the sliding surfaces were seen to vanish, with consequent uplift of the superstructure, when the friction pendulum system was subjected to the El Centro three-directional record [6]. However, no uplift occurred when the vertical ground acceleration was excluded from the analysis. Therefore, for the El Centro

© The 17th World Conference on Earthquake Engineering

case only, the displacement response spectra were computed considering simultaneous action of the two horizontal components only. The results presented in the companion paper, [6], are shown again in the following subsections and extended to include base shear, residual displacement, seismic input energy and distance traveled by the FP slider.

Table 1. Characteristics of ground motions considered

Earthquake	Year	M	Station	e_d (km)	t_d (s)	Type
Mexico City	1985	8.1	SCT	400	54	Far-source long-period
Chuetsu-Oki	2007	6.8	Kashiwazaki NIG018	21	7	Near-source long-period
Iwate-Miyagi Nairiku	2008	7.2	Naruko MYG005	32	36	Near-source long-period?
Imperial Valley	1979	6.5	El Centro (Array Sta 6)	3.5*	6	Near-source long-period

*For the El Centro record only, e_d indicates the closest distance to the fault.

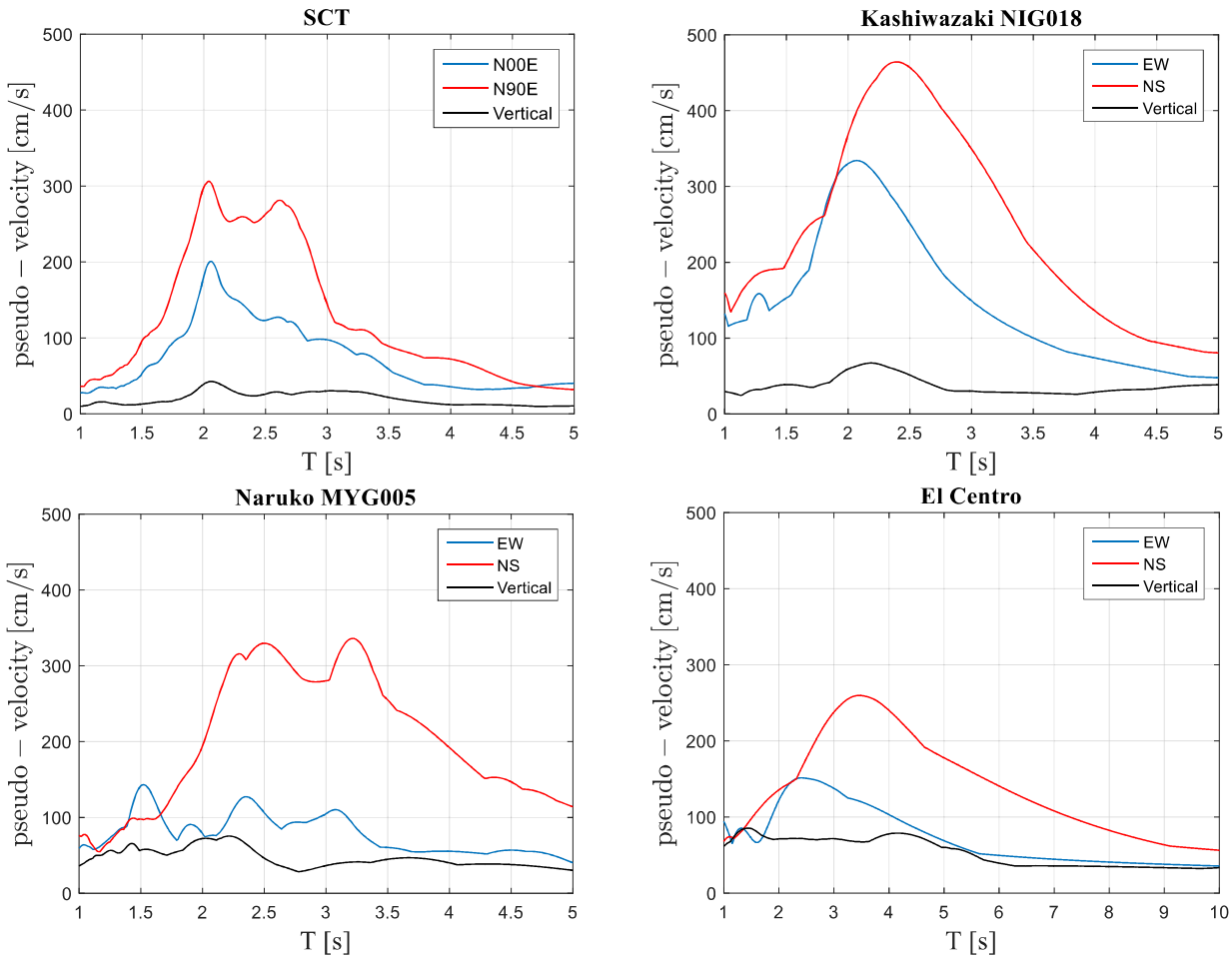

Fig. 1 – Pseudo-velocity response spectra for damping ratio ζ=0.05

3.1 Maximum displacement

The displacement response spectra for values of the friction coefficient, μ, varying between 0.03 and 0.10, are plotted in Fig.2 for each of the four earthquakes considered. The norm of the horizontal displacement vector, $\mathbf{r}_h$, normalized with respect to the radius of curvature, R, is shown in the spectra. Three values of

© The 17th World Conference on Earthquake Engineering

$\|\mathbf{r}_h\|/R$ are denoted by thick horizontal lines in Fig.2, namely 0.1, 0.2 and 0.3. The value of 0.1 indicates the onset of nonlinear behavior, 0.2 is a typical design limit, while 0.3 represents that value below which the error associated with the use of a geometrically linear response theory is generally still considered acceptable. We note that for a wide range of periods the earthquake displacement demands are way beyond the capacity of the isolation devices currently used.

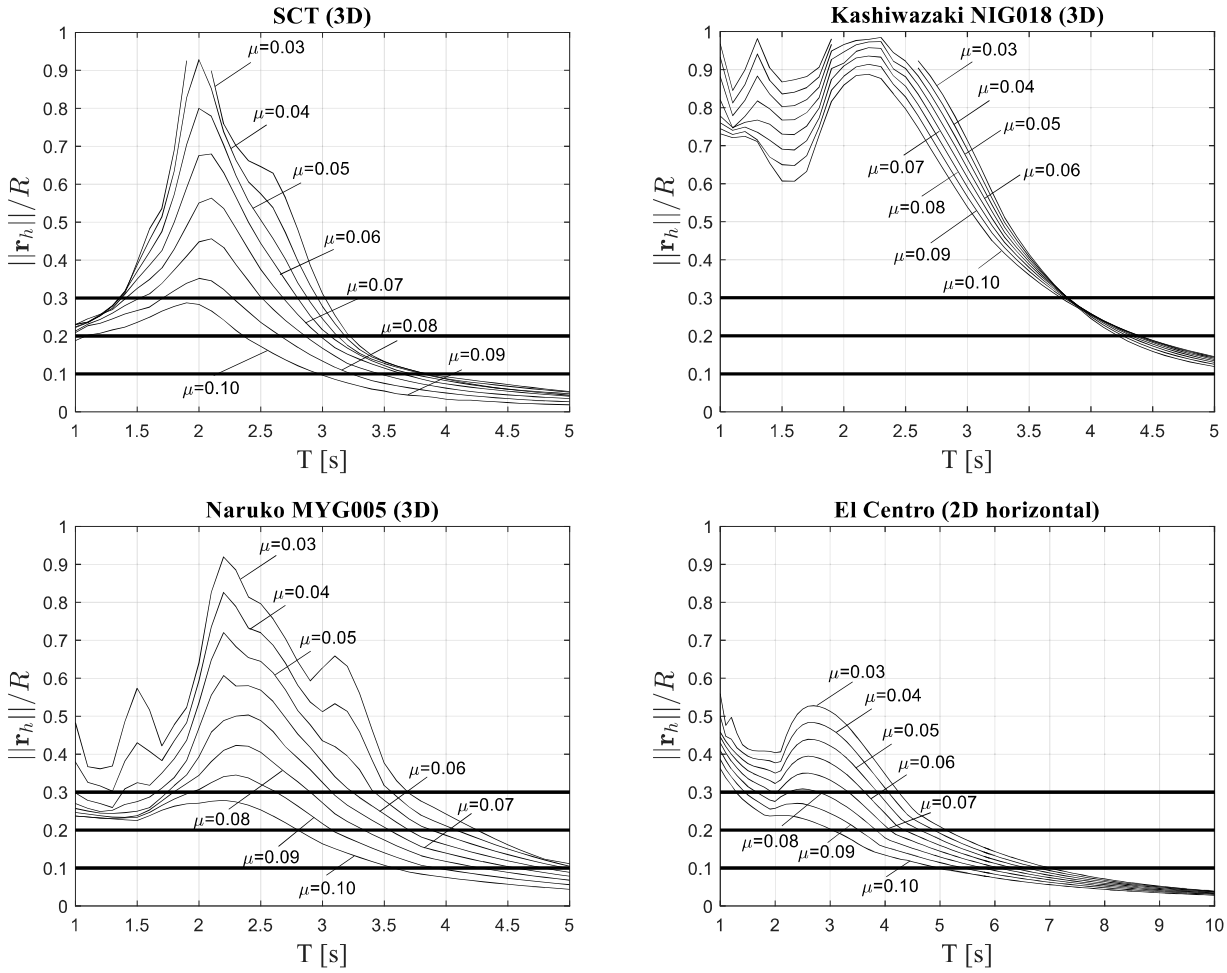

Fig. 2 – Horizontal displacement response spectra

3.2 Maximum base shear

The displacement response spectra may be used to determine the combination of period, T, and coefficient of friction, μ, that the isolation system should be designed for to guarantee that the maximum allowable displacement is not exceeded. However, the effectiveness of a base isolation system is measured based on its ability to reduce the base shear and the earthquake-induced forces in the superstructure. The base shear response spectra for values of the friction coefficient, μ, varying between 0.03 and 0.10, are plotted in Fig.3 for each of the four earthquakes considered. The norm of the horizontal force vector, $\|\mathbf{F}_h\|$, normalized with respect to the weight of the superstructure, $W=mg$, is shown in the spectra. For small displacements ($\|\mathbf{r}_h\|/R \ll 1$), the maximum lateral seismic force acting on a friction pendulum system may be written as

$$V_b = \mu W + \frac{W}{R} D_M \tag{11}$$

© The 17th World Conference on Earthquake Engineering

where D_M is the design maximum displacement of the isolation system. Dividing both sides of Eq. (11) by the weight of the superstructure, W, gives the following expression for the base shear coefficient:

$$\frac{V_b}{W} = \mu + \frac{D_M}{R} \tag{12}$$

Computed using Eq. (12), with a friction coefficient μ=0.1 and values of the maximum displacement, D_M, equal to 0.1R, 0.2R and 0.3R respectively, three values of $\|\mathbf{F}_h\|/mg$ are denoted by thick horizontal lines in Fig.3, namely 0.2, 0.3 and 0.4. We note that for lower values of the friction coefficient, μ, such lines would be lower. For instance, if μ=0.03, the three base shear coefficients, $\|\mathbf{F}_h\|/mg$, would be 0.13, 0.23 and 0.33. As already seen for isolator displacements, the seismic demands in terms of base shear are also unacceptably high in a wide range of periods.

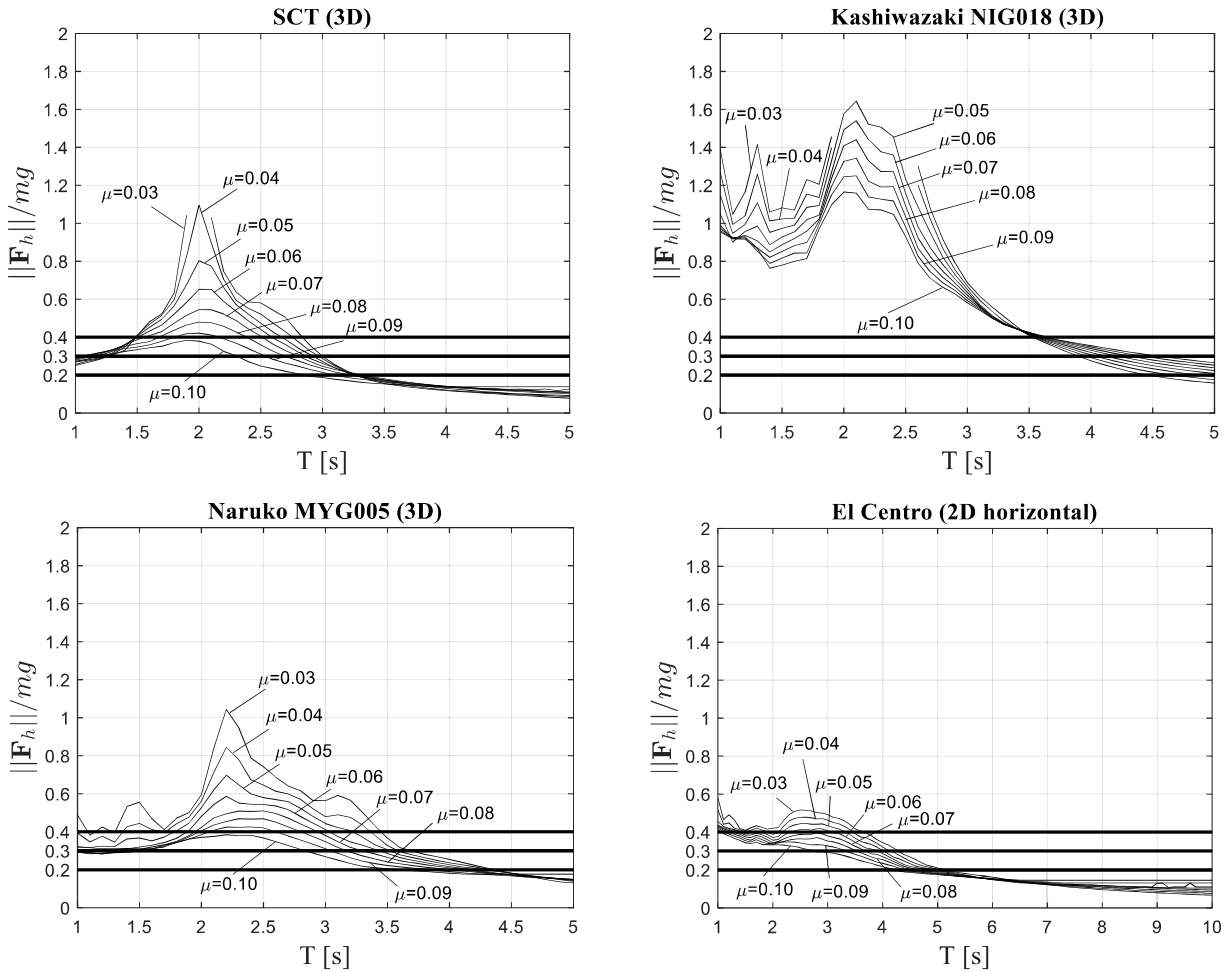

Fig. 3 – Base shear response spectra

3.3 Residual displacement

Experimental [8] and analytical studies [9] have shown that base-isolated structures can exhibit significant post-earthquake residual displacements. These may affect the serviceability of the structure and compromise the functionality of structural and nonstructural elements crossing the isolation plane. Since it may not always be possible to re-center an isolation system after an earthquake, it is important to predict the potential

© The 17th World Conference on Earthquake Engineering

residual displacement so that the structure can be designed to accommodate the permanent offset. As a result, recommendations are provided in building codes to estimate permanent residual displacements in isolation systems [10]. Theoretically, it can be shown that the residual displacement cannot be greater than μR. The norm of the residual displacement vector, $\|\mathbf{r}_h\|_{res}$, normalized with respect to μR, is plotted in Fig.4 for each of the four earthquakes considered. While the plots confirm that the residual displacement is always smaller than μR, they also suggest that the response in terms of residual displacements is chaotic rather than exhibiting a well-defined and predictable behavior. We observe that based on the formula prescribed in [10], the maximum expected residual displacement would be $0.16\mu R$ (red horizontal lines in Fig.4). As shown in Fig.4, most of the residual displacements computed under the 4 earthquakes considered are much larger than that value. However, we note that the formula in [10] is based on linear kinematics while the results in Fig.4 were obtained considering a geometrically nonlinear friction pendulum model with horizontal and vertical displacements virtually as high as the radius of curvature, R, of the sliding surface.

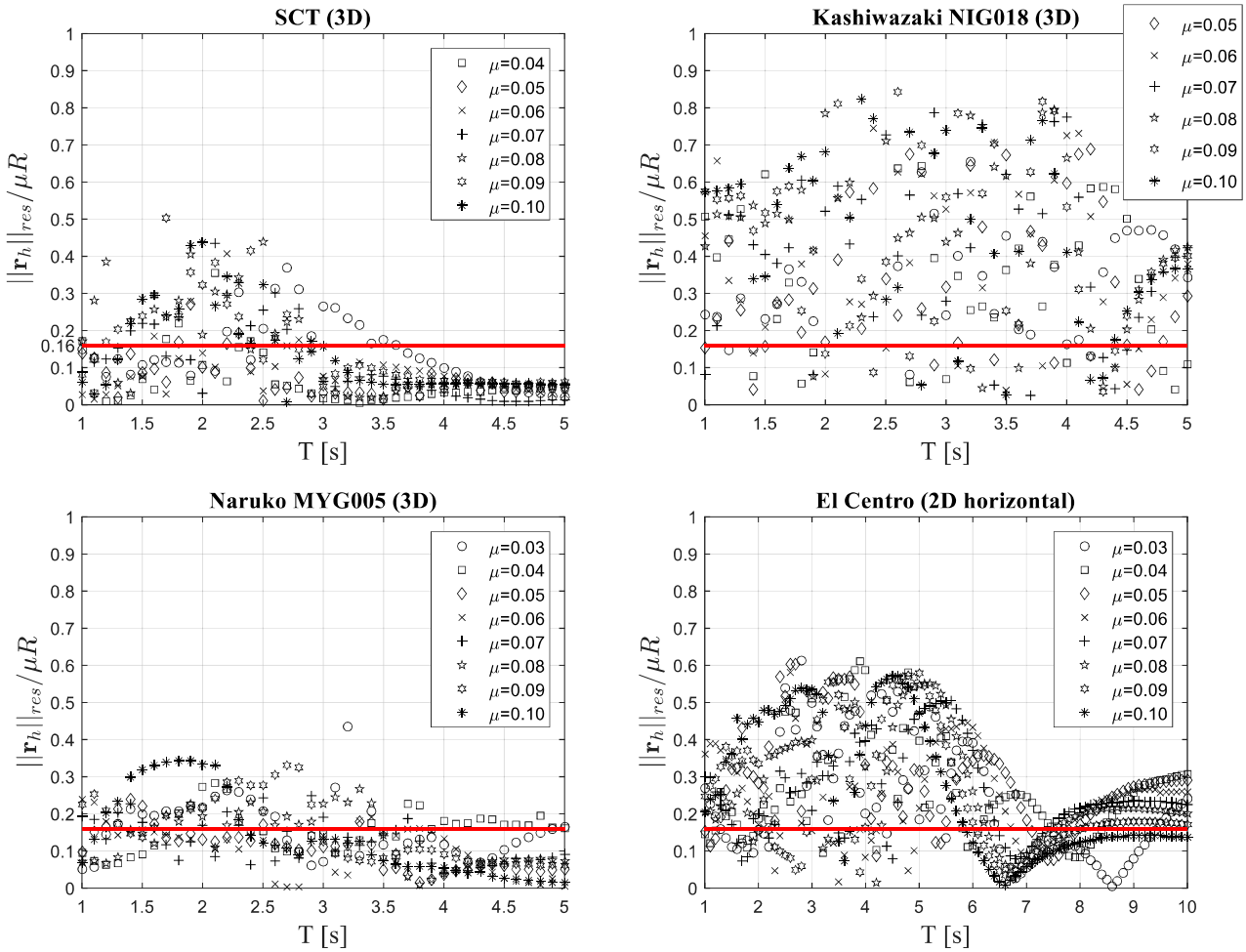

Fig. 4 – Residual displacements

3.4 Seismic input energy

In earthquake building codes in Japan, the response prediction method based on energy balance is a popular approach to determine the response of seismically isolated buildings [11]. Seismic input energy, E_I, is a basic design quantity of such method and design energy spectra are determined by converting E_I into equivalent velocity

© The 17th World Conference on Earthquake Engineering

$$V_E = \sqrt{\frac{2E_I}{m}} \tag{13}$$

Computed using Eq. (3) and Eq. (13), the energy spectra for values of the friction coefficient, μ, varying between 0.03 and 0.10, are plotted in Fig.5 for each of the four earthquakes considered.

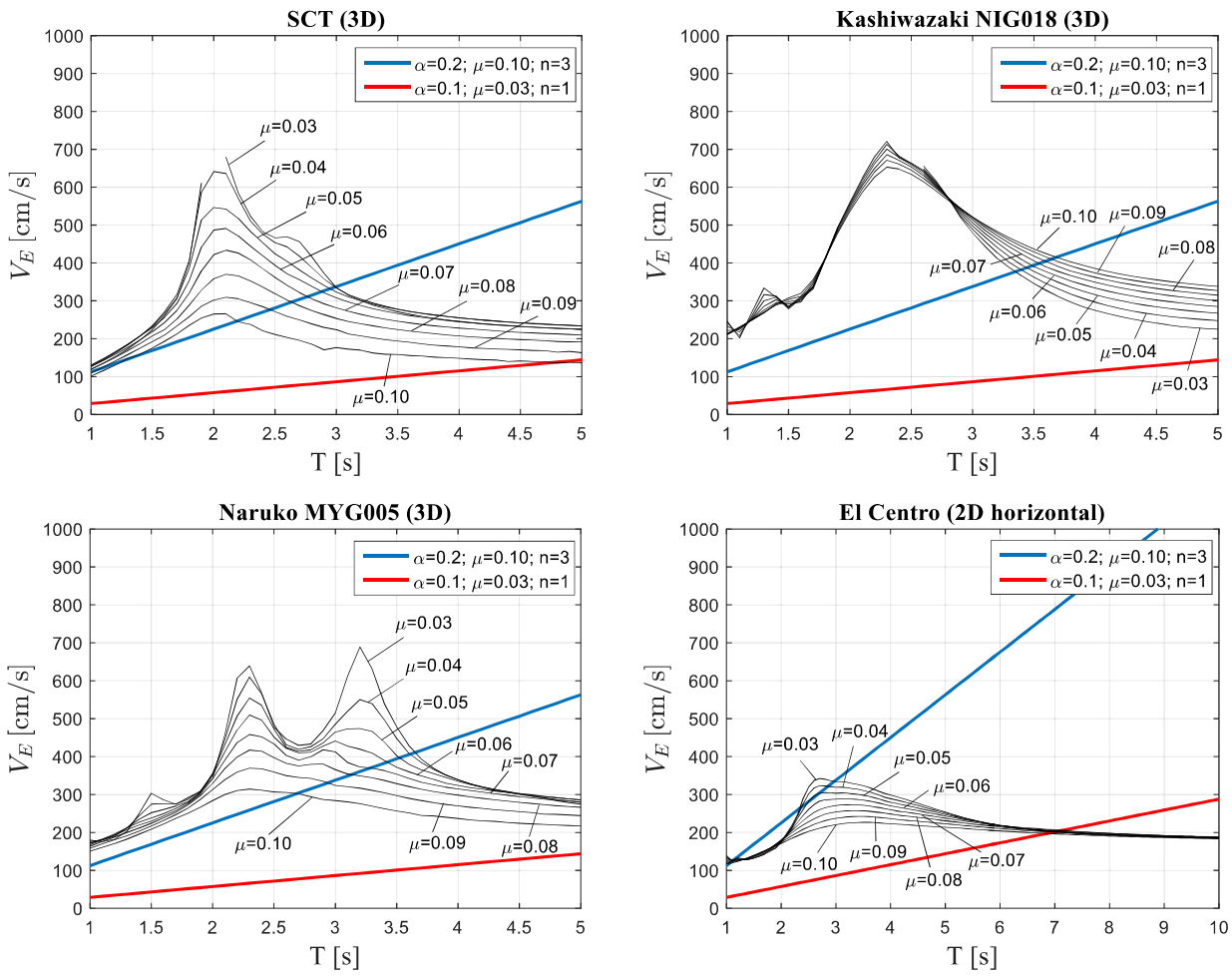

Fig. 5 – Input energy spectra

For convenience, we write the maximum displacement, D_M, as a function of the radius of curvature, R, as follows

$$D_M = \alpha R \tag{14}$$

The energy, E_A, that the system is capable of absorbing in n cycles of vibration at the design maximum displacement, D_M, is given by

$$E_A = \frac{1}{2}\frac{W}{R}D_M^2 + 4\mu W D_M n \tag{15}$$

© The 17th World Conference on Earthquake Engineering

where the first term is the elastic strain energy and the second term is the energy dissipated by friction. Eq. (15) may also be used to define the maximum energy capacity of the system under an earthquake. Substituting Eq. (14) into Eq. (15), and converting E_A into equivalent velocity, V_E, gives

$$V_E = \sqrt{\alpha(\alpha + 8\mu n) gR} \tag{16}$$

Computed using Eq. (16), two lines are plotted in Fig.5, representing different energy capacity levels of the system. The lower red line was computed using α=0.1, μ=0.03 and n=1, while the upper blue line was obtained using α=0.2, μ=0.10 and n=3. Clearly, the higher the number of cycles, n, at maximum displacement, $D_M=\alpha R$, the higher the energy capacity of the system and the longer the distance traveled by the slider. Fig.5 shows that the seismic demands on the isolation system exceed by far the assumed capacity in a wide range of periods.

3.5 Traveled sliding distance

An additional measure of the seismic demand on the isolation system is given by the distance, d_S, traveled by the friction pendulum slider. This can be easily computed as

$$d_S = \int_0^{t_F} \|\dot{\mathbf{r}}\| dt \tag{17}$$

where t_F is the total duration of the ground motion and $\dot{\mathbf{r}}=\dot{\mathbf{r}}_h+\dot{z}\mathbf{e}_z$. For the detailed expression of $\dot{\mathbf{r}}$, the reader is referred to [6]. The traveled sliding distance spectra, for values of the friction coefficient, μ, varying between 0.03 and 0.10, are plotted in Fig.6 for each of the four earthquakes considered. The distance traveled by the slider is related to the energy dissipation of the device. For a design displacement, $D_M=\alpha R$, and a capacity of the isolator to complete n cycles at that displacement, the traveled distance, d_s, would be

$$d_s = 4D_M n = 4\alpha R n \tag{18}$$

By expressing the radius of curvature as a function of period, T, Eq. (18) becomes

$$d_s = 4\alpha n \left(\frac{T}{2\pi}\right)^2 g \tag{19}$$

Computed using Eq. (19), two curves are plotted in Fig.6, representing different levels of maximum sliding distance capacity. The lower red line was computed using α=0.2 and n=1, while the upper blue line was obtained using α=0.2 and n=3. As seen earlier for other response quantities, in this case too demand exceeds capacity in a wide range of periods.

4. Conclusions

This work was motivated by the fact that friction-based systems can exhibit an unbounded response at resonance and they are therefore especially vulnerable to quasi-periodic long duration earthquakes, as was the 1985 Mexico City earthquake. Particularly dangerous are also near-fault long-period ground motions, such as Imperial Valley 1979 and Chuetsu-Oki 2007. These may exhibit large vertical accelerations that can cause the normal force on the isolators to vanish with uplift of the superstructure and subsequent impact.

© The 17th World Conference on Earthquake Engineering

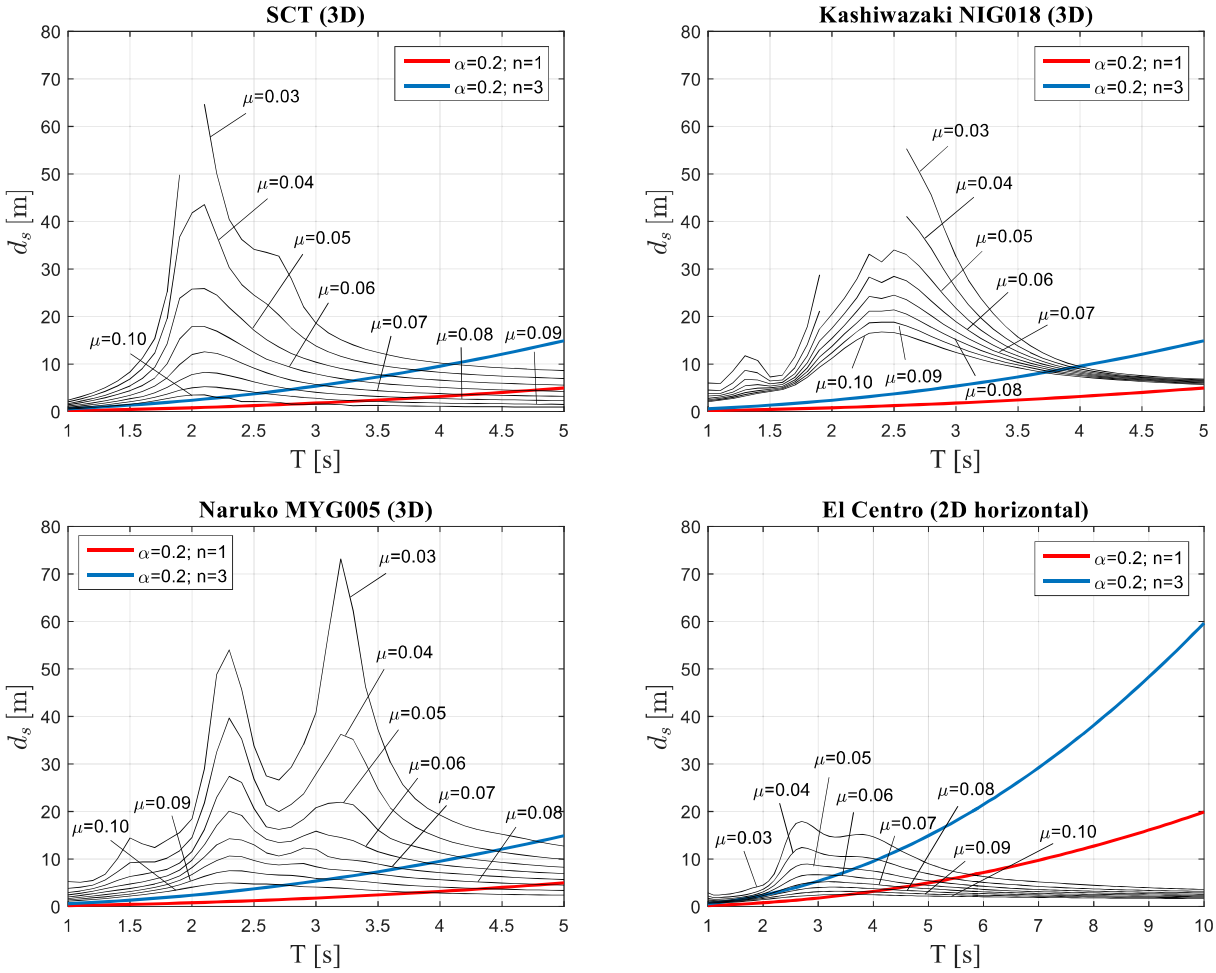

Fig. 6 – Traveled sliding distance, d_s, as a function of isolation period T

In a companion paper [6], a three-dimensional formulation was presented for the dynamic analysis of FP systems including large oscillations and the inherent nonlinearities related to the motion of a mass sliding with friction on a sphere.

In the present paper, such a formulation has been used to determine the demands of four extreme earthquake motions on friction pendulum systems of varying period and coefficient of friction. The three components of each ground motion were applied simultaneously and five relevant response quantities were considered: isolator displacement, base shear coefficient, residual displacement, input energy and slider traveled distance. For all these quantities, the seismic demands are seen to exceed the isolation system capacity, evaluated on the basis of current design assumptions, in a wide range of periods.

Keeping in mind that the use of friction pendulum systems may not be appropriate when earthquakes as those used in this study are expected, it may be worthwhile investigating the response of FP systems with longer periods than those considered here.

5. References

[1] Den Hartog JP. LXXIII (1930): Forced vibrations with combined viscous and coulomb damping. *The London, Edinburgh, and Dublin Philosophical Magazine and Journal of Science*, **9** (59), 801-817.

[2] Den Hartog JP, Mikina SJ (1932): Forced vibrations with nonlinear springs. *Transactions of the American Society of Mechanical Engineers (ASME)*, **54**, 157-164.

© The 17th World Conference on Earthquake Engineering

[3] Den Hartog JP (1984): *Mechanical vibrations*. New York: Dover Publications, Inc.

[4] Chopra AK (2012): *Dynamics of Structures*. Prentice Hall: New Jersey.

[5] Oliveto ND (2020): Nonlinear dynamic analysis of curved surface slider systems under harmonic, near-fault and long-period ground motions. *Journal of Engineering Mechanics (ASCE)*, **146** (9), 04020087.

[6] Oliveto ND (2020): 3D analysis of friction pendulum systems under near-fault and long-period ground motions. *17th World Conference on Earthquake Engineering*, *17 WCEE*, Sendai, Japan.

[7] Trifunac MD, Brady AG (1975): A Study on the Duration of Strong Earthquake Ground Motion. *Bulletin of the Seismological Society of America*. **65** (3), 581-626.

[8] Ryan KL, Coria CB, Dao ND (2012): Large scale earthquake simulation for hybrid lead rubber isolation system designed with consideration for nuclear seismicity. U.S. Nuclear Regulatory Commission CCEER 13-09.

[9] Katsaras A (2008): Evaluation of current code requirements for displacement restoring capability of seismic isolation systems and proposals for revisions. Project No. GOCE-CT-2003-505488, LessLoss Project cofounded by European Commission with 6th Framework.

[10] ASCE/SEI 7-16 (2017): Minimum Design Loads and Associated Criteria for Buildings and Other Structures. *American Society of Civil Engineers*, Reston, VA, USA.

[11] Architectural Institute of Japan (AIJ) (2016): Design recommendations for seismically isolated buildings. Committee for Seismically Isolated Structures, Japan.

© The 17th World Conference on Earthquake Engineering